Chiral superconductivity in thin films of doped Bi_2Se_3

Luca Chirolli*
IMDEA-Nanoscience, Calle Faraday 9, E-28049 Madrid, Spain

(Received 2 March 2018; revised manuscript received 18 May 2018; published 9 July 2018)

Recent experimental evidences point to rotation symmetry-breaking superconductivity in doped Bi_2Se_3, where the relevant order parameter belongs to a two-component odd-parity representation E_u of the crystal point group. The E_u channel admits two possible phases, the nematic phase, that well explains the reported rotation symmetry breaking, and the chiral phase, that breaks time-reversal symmetry. In weakly anisotropic three-dimensional (3D) systems the nematic phase is the stable one. We study the stability of the nematic phase versus the chiral phase as a function of the anisotropy of the Fermi surface and the thickness of the sample and show that by increasing the 2D character of the Fermi surface or by reducing the number of layers in thin slabs the chiral phases is favored. For the extreme 2D limit composed by a single layer of Bi_2Se_3 the chiral phase is always the stable one and the system hosts two chiral Majorana modes flowing at the boundary of the system.

DOI: 10.1103/PhysRevB.98.014505

I. INTRODUCTION

Chiral superconductivity is a topological quantum state of matter in which an unconventional superconductor spontaneously breaks time-reversal symmetry and develops an intrinsic angular momentum [1]. Its peculiar gap structure realizes a triplet $p_x + ip_y$ state that is topologically nontrivial. Key signatures in two-dimensional (2D) systems are chiral Majorana edge modes and Majorana zero energy states in vortex cores [2–7]. In three dimensions, chiral superconductivity (SC) is also possible, allowing the realization of a Weyl superconductor with Majorana arcs on the surface [8–10]. A possible candidate material for hosting this superconducting state is SrPtAs [11,12]. Chiral superconductors have attracted great interest for their unconventional character and their potential use in the field of quantum computation [13,14].

Recently, strong experimental evidences of unconventional superconductivity have been reported for a well-known material, Bi_2Se_3, that in its pristine form is a topological insulator (TI) [15,16]. Possibly odd-parity superconductivity was first reported in Bi_2Se_3 intercalated with Cu [17–19], although clear evidence for the characteristic surface Andreev states has remained controversial [20–22]. The first studies motivated the theoretical characterization of 3D, time-reversal invariant (TRI) topological superconductivity in centrosymmetric systems [23]. A much richer phenomenology has recently emerged, showing a broken C_3 symmetry in the superconducting state in samples intercalated with Cu, Nb, and Sr [24–27]. Several experiments reported uniaxial anisotropy response to an in-plane magnetic field in the Knight shift [28], the upper critical field [29,30], the magnetic torque [27], and the specific heat [29]. Specific heat [19] and penetration depth [31,32] have excluded the presence of line nodes on the Fermi surface. All these observations support a pairing state of nematic type belonging to the two-component representation E_u of the crystal point group [33,34].

Theoretical modeling has also addressed different aspects of the E_u states from bulk properties [35–37] to surface states [10], vortex states [38,39], the interplay between E_u superconductivity and magnetism in promoting time-reversal symmetry-breaking states [40,41], and the role of odd-parity fluctuations as the mechanism at the basis of E_u superconductivity [42] and preemptive nematicity above T_c [43,44].

In this work we study superconductivity in Bi_2Se_3 in the E_u odd-parity channel, focusing on the stability of the nematic phase versus the chiral phase as a function of the anisotropy of the system and the thickness of the sample. Bi_2Se_3 is a layered material in which the unit cell is constituted by a quintuple layer (QL) structure. It is therefore reasonable to study the behavior of the system by varying the interlayer coupling and the chemical potential. We show that an increase of the two-dimensional character of the Fermi surface favors the chiral phase. Chemical dopants intercalate between the unit cells and modify their distance and relative coupling, together with the charge density. Strong anisotropy can be achieved by increasing the doping or by properly choosing the dopants so to increase the interlayer spacing of the materials.

Interestingly, a second root towards chiral superconductivity is provided by exfoliation. In particular, the chiral phase is the natural phase of the E_u channel in the extreme 2D limit of a single layer [33,34]. We show that by reducing the thickness of the sample without increasing the anisotropy of the system naturally drives the system towards the chiral phase. We find as a rough estimate that a thin slabs with approximately 10 layers marks the stability threshold between the nematic and the chiral phase. Experimentally, exfoliation down to the single QL case has been achieved [45,46], making this root a promising way toward chiral quasi-2D superconductors.

The single-layer case acquires high relevance in the context of 2D materials engineering, whereby properties of a material can be fine-tuned by coupling with a proper substrate. By placing a single layer of Bi_2Se_3 on top of a suitable substrate,

*luca.chirolli@imdea.org

the planar mirror inversion symmetry breaks explicitly, the point group is reduced to C_{3v}, and the system is expected to show Rashba spin-orbit interaction. This possibility becomes highly relevant in the light of recent theoretical developments concerning time-reversal symmetry breaking in 2D noncentrosymmetric systems [47], according to which the superconducting state can break time-reversal symmetry only in the presence of a threefold rotation symmetry. As shown in Ref. [47], if the superconducting order parameter belongs to the E_u representation the chiral state must appear for sufficiently large Rashba coupling. This implies that the SC order parameter only gradually changes as the surface Rashba coupling is included, even if the Kramers degeneracy is lifted. These considerations boost single layers of Bi_2Se_3 as an optimal candidate for the observation of chiral superconductivity in 2D systems.

The realization of the chiral state promotes the system to class D topological superconductors that in 2D are characterized by a $\mathbb{Z}$ topological invariant and are expected to show chiral Majorana modes flowing at the boundary [48]. The number of chiral Majorana modes is dictated by the Chern number, that in the present case takes the value $C_{\rm ch} = \pm 2$ for the $p_x \mp i p_y$ solution. Starting from a tight-binding model that well approximates the complicated band structure of Bi_2Se_3, we show that the chiral phase in this material supports two chiral Majorana modes that copropagate at the boundary of the system and can find useful applications in interferometric schemes [49]. The low-energy Hamiltonian of the system is a massive Dirac Hamiltonian, so our results apply to generic systems that share the same low-energy description, such as TI thin films [50] and Rashba bilayer system [51].

The work is structured as follows: In Sec. II we review the known analysis of the two-component superconducting channel of the D_{3d} crystal point group. In Sec. III we derive the Ginzburg-Landau function that describes the condensation of the two-component channel. In Sec. IV we study the stability of the chiral phase and show that in the strong anisotropic case it is the favored phase. In Sec. V we show that by reducing the thickness of the sample a chiral phase is obtained for thin slabs. In Sec. VI we study the surface states through a tight-binding numerical simulation. Finally, in Sec. VII we conclude with a summary of the results.

II. E_u SUPERCONDUCTIVITY

We consider doped Bi_2Se_3 in the $k \cdot p$ low-energy approximation introduced in Ref. [23]. The point group of the crystal is D_{3d} and the system can be described by a simplified model in which the unit cell is constituted by a bilayer structure where spin s electrons occupy p_z-like orbitals on the top (T) and bottom (B) layers of the microscopic QL unit cell. The low-energy Hamiltonian is described by a massive anisotropic ($v_z \neq v$) Dirac model that reads

$$H^0_{\mathbf{k}} = m\sigma_x + v(k_x s_y - k_y s_x)\sigma_z + v_z k_z \sigma_y, \tag{1}$$

where Pauli matrices σ_i and s_i describe the orbital and spin degrees of freedom, respectively. The Hamiltonian is TRI, where the time reversal operator is $\mathcal{T} = i s_y K$ with K complex conjugation.

Superconductivity is described within the Bogoliubov–de Gennes (BdG) formalism by introducing the Nambu spinor $\Psi_{\mathbf{k}} = (\mathbf{c}_{\mathbf{k}}, i s_y \mathbf{c}^\dagger_{-\mathbf{k}})^T$, with $\mathbf{c}_{\mathbf{k}}$ fermionic annihilation operators of the Hamiltonian $H^0_{\mathbf{k}}$. The Hamiltonian reads $\hat{\mathcal{H}} = \frac{1}{2}\int d\mathbf{k} \Psi^\dagger_{\mathbf{k}} H(\mathbf{k}) \Psi_{\mathbf{k}}$, with

$$H_{\mathbf{k}} = \left(H^0_{\mathbf{k}} - \mu\right)\tau_z + \Delta_{\mathbf{k}}\tau_+ + \Delta^\dagger_{\mathbf{k}}\tau_-, \tag{2}$$

and with $\Delta_{\mathbf{k}}$ generic momentum-dependent 4×4 gap matrices. The Nambu construction imposes that $H_{\mathbf{k}}$ has a charge conjugation symmetry $\mathcal{C}$ implemented as $U_{\mathcal{C}} H(-\mathbf{k})^* U^\dagger_{\mathcal{C}} = -H(\mathbf{k})$, with $U_{\mathcal{C}} = s_y \tau_y$. $\mathcal{C}$ imposes a restriction on the pairing matrix, $s_y \Delta^*(-\mathbf{k}) s_y = \Delta(\mathbf{k})$. If pairing is momentum independent, there are only six possible matrices in the irreducible representations of the D_{3d} point group that satisfy this constraint and they have been classified in Ref. [23]. Accordingly, they are given by the even-parity channel I and σ_x belonging to the A_{1g} representation, the odd-parity channel $\sigma_y s_z$ belonging to A_{1u} representation, σ_z belonging to the A_{2u} representation, and $(-\sigma_y s_y, \sigma_y s_x)$ belonging to the E_u representation. In particular, the latter forms a two-component representation that can describe nematic or chiral SC [33,34].

Focusing on the E_u odd-parity channel we associate to the matrix operators the following order parameters:

$$\boldsymbol{\psi} = (\psi_x, \psi_y) \sim (-\sigma_y s_y, \sigma_y s_x) \sim E_u.$$

In Ref. [23] it was shown that when only local pairing is considered, the A_{1u} is the leading instability in a wide range of parameters in the phase diagram. On the other hand, the author has shown that inclusion of momentum-dependent pairing terms only affects the critical temperature of the nematic channel E_u [40], rising it with respect to the critical temperature of the A_{1u} channel. Recently, odd-parity fluctuations together with repulsive Coulomb interactions have also emerged as a possible mechanism that selects the E_u odd-parity two-component channel as the leading SC channel [42]. We then assume that the nematic channel condenses and focus on the competition between the nematic and chiral phases.

III. GINZBURG-LANDAU THEORY

We start considering the E_u phase $\boldsymbol{\psi}$ and study the conditions under which a chiral phase occurs. Symmetry dictates the form of its free energy that reads

$$F_\psi = a|\boldsymbol{\psi}|^2 + b_1|\boldsymbol{\psi}|^4 + b_2|\psi_x \psi^*_y - \psi_y \psi^*_x|^2. \tag{3}$$

The E_u representation admits two possible superconducting states: a nematic state $\boldsymbol{\psi} \propto (1,0)$ which is time-reversal invariant and has point nodes on the equator of the Fermi surface and a chiral state $\boldsymbol{\psi} \propto (1,i)$ which breaks TR symmetry and has $C = \pm 2$ Weyl nodes at the north and south pole of the Fermi surface [34]. The sign of the coupling b_2 determines whether the E_u representation chooses the nematic (for $b_2 > 0$) or the chiral state (for $b_2 < 0$). Microscopic calculations show that for a 3D isotropic model $b_2 > 0$, so that no TRB phase may arise in the system [33,34]. We now specifically study the sign of the coupling b_2 versus Fermi surface anisotropy and sample thickness.

Setting the chemical potential in the conduction band, $\mu > m$, we can reduce the dimensionality of the problem by

projecting the Hamiltonian and the gap matrix down to the conduction band, so that the gap matrix reads

$$\Delta_{\mathbf{k}} = \psi_x \mathbf{d}_x \cdot \tilde{\mathbf{s}} + \psi_y \mathbf{d}_y \cdot \tilde{\mathbf{s}}, \tag{4}$$

where $\mathbf{d}_x = (0, -\tilde{k}_z, \tilde{k}_y)$ and $\mathbf{d}_y = (\tilde{k}_z, 0, -\tilde{k}_x)$, the momentum has been rescaled as $\tilde{\mathbf{k}} = (vk_x, vk_y, v_z k_z)/\mu$, and $\tilde{\mathbf{s}}$ is a momentum-dependent spin-1/2 like vector operator parametrizing the twofold-degenerate subspace at every $\mathbf{k}$ point associated to Kramers degeneracy [52]. Explicitly, defining $|\psi_{\mathbf{k},1}\rangle$ and $|\psi_{\mathbf{k},2}\rangle$ the two degenerate eigenstates in the conduction band at momentum $\mathbf{k}$, the vector $\tilde{\mathbf{s}}$ is obtained as $\tilde{s}_x = |\psi_{1,\mathbf{k}}\rangle\langle\psi_{2,\mathbf{k}}| + \text{H.c.}$, $\tilde{s}_y = -i|\psi_{1,\mathbf{k}}\rangle\langle\psi_{2,\mathbf{k}}| + \text{H.c.}$, and $\tilde{s}_z = |\psi_{1,\mathbf{k}}\rangle\langle\psi_{1,\mathbf{k}}| - |\psi_{2,\mathbf{k}}\rangle\langle\psi_{2,\mathbf{k}}|$.

We can now integrate away the fermionic degrees of freedom and obtain a nonlinear functional for the order parameters

$$\mathcal{S} = \int_0^\beta d\tau \frac{1}{V} \text{Tr}[\hat{\Delta}^\dagger \hat{\Delta}] - \frac{1}{\beta} \text{Tr} \ln\left(-\mathcal{G}_0^{-1} + \Sigma\right), \tag{5}$$

with $-\mathcal{G}_0^{-1} = \partial_\tau + (H_0 - \mu)\tau_z$, $\Sigma = \tau_+ \hat{\Delta} + \tau_- \hat{\Delta}^\dagger$, $\beta = 1/T$ the inverse temperature, and the trace is over all the degrees of freedom, $\text{Tr} \equiv T \sum_\omega \int d\mathbf{k}$. As usual, the microscopic GL theory is obtained by expanding the nonlinear action in powers of the fields,

$$\text{Tr} \ln\left(-\mathcal{G}_0^{-1} + \Sigma\right) = \text{Tr} \ln\left(-\mathcal{G}_0^{-1}\right) - \sum_{n=1}^{\infty} \frac{1}{n} \text{Tr}(\mathcal{G}_0 \Sigma)^n. \tag{6}$$

The fourth-order coefficient are determined by the fourth-order averages $\langle \Delta_{\mathbf{k}} \Delta^*_{\mathbf{k}} \Delta_{\mathbf{k}} \Delta^*_{\mathbf{k}} \rangle$, where $\langle \ldots \rangle = T \sum_{\omega_n} \int \frac{d\mathbf{k}}{(2\pi)^3} G_+^2 G_-^2 \text{Tr}[\ldots]$, $G_\pm = (i\omega_n \mp \xi_{\mathbf{k}})^{-1}$, $\xi_{\mathbf{k}} = \epsilon_{\mathbf{k}} - \mu$, and $\epsilon_{\mathbf{k}} = \sqrt{\mu^2 \tilde{\mathbf{k}}^2 + m^2}$ is the dispersion of the conduction band. Explicitly, the fourth-order terms are given by

$$b_1 = 3\langle (\mathbf{d}_x \cdot \mathbf{d}_y)^2 \rangle + \langle (\mathbf{d}_x \times \mathbf{d}_y)^2 \rangle, \tag{7}$$

$$b_2 = -\langle (\mathbf{d}_x \cdot \mathbf{d}_y)^2 \rangle + \langle (\mathbf{d}_x \times \mathbf{d}_y)^2 \rangle. \tag{8}$$

Clearly, parallel vectors $\mathbf{d}_i$ favor a chiral phase and orthogonal vectors favor a nematic phase.

IV. CHIRAL PHASE FOR STRONG ANISOTROPY

We now study the parameter b_2 as a function of the anisotropy of the Fermi surface. By performing the averages one can approximate

$$b_2 = \kappa \int d^3\tilde{k} \left[\tilde{k}_z^2 \left(\tilde{k}^2 + \tilde{k}_z^2\right) - \tilde{k}^4/8\right] \delta(\xi_{\tilde{\mathbf{k}}}/\mu), \tag{9}$$

where $\kappa = 7\zeta(3) N_F/[8(\pi T_c)^2]$, $N_F = \int d^3\mathbf{k} \delta(\xi_{\mathbf{k}})/(2\pi)^3$ the density of states at the Fermi level, and $\tilde{k}^2 = \tilde{k}_x^2 + \tilde{k}_y^2$. For an isotropic Fermi surface the coefficient b_2 is positive and the nematic phase is favored. By inspection of Eq. (9) it becomes clear how a strong anisotropy of the Fermi surface can drive the system into the $b_2 < 0$ regime.

The Hamiltonian Eq. (1) is linear in momentum and characteristic surface states of the TI arise when $\text{sign}(mv_z) < 0$ for states confined in $z > 0$ [53]. Nevertheless, quadratic corrections in the mass term can be also considered and appear in more refined band structure calculations [15],

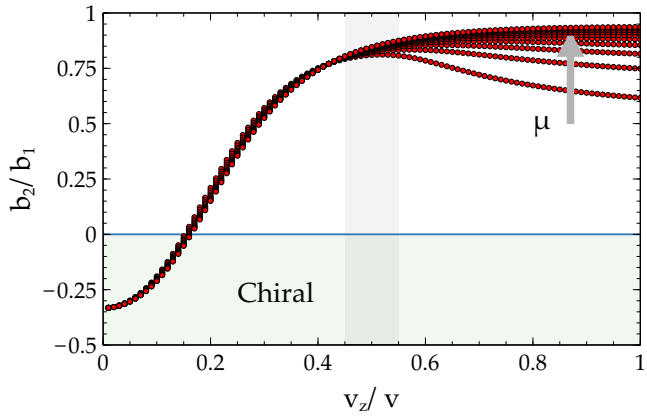

FIG. 1. Variation of the coefficient ratio b_2/b_1 as a function of the anisotropy of the system parametrized by v_z/v and the chemical potential μ, keeping the parameter α_z fixed. For sufficiently small v_z/v the coefficient b_2 becomes negative ($b_1 > 0$) and the chiral phase becomes possible.

$$m(\mathbf{k}) = m - \alpha k^2 - \alpha_z k_z^2, \tag{10}$$

where $k^2 = k_x^2 + k_y^2$. For $m, \alpha, \alpha_z > 0$ the mass term changes sign on a particular surface in momentum space. This property yields a nontrivial topology of the insulator. For simplicity, we neglect a spin- and orbital-independent term that adds to the Hamiltonian as a diagonal $\mathbf{k}$-dependent contribution and does not change the topological properties of the system, a part from breaking the particle-hole symmetry of the Dirac Hamiltonian describing the topological insulator.

The momentum dependence of the mass term introduces a second scale α_z along the k_z direction that, together with the velocity v_z, makes the Fermi surface intrinsically anisotropic. If α_z is neglected, the unique scale v_z can be reabsorbed into a redefinition of the momentum and it eventually factorizes in the expression of b_1 and b_2 in a way that their value become fixed and positive. It is then reasonable to study the parameter b_2 as we increase the anisotropy of the Fermi surface by considering finite α_z.

The values of v_z and α_z can be controlled by chemical doping, in that dopants intercalate between the QLs and modify the interlayer distance a_z and hopping t_z. The latter can be assumed to be exponentially dependent on a_z itself, $t_z = t_z^0 \exp(-a_z/R)$, with R a microscopic length scale characteristic of the p_z orbital of Se, and t_z^0 the amplitude of the hopping integral. It then follows that an increase in the doping is expected to lower both v_z and α_z.

In Fig. 1 we plot the dependence of b_2/b_1 as a function of v_z/v, keeping α_z constant and taking for reference the parameters of the well-known model of Ref. [15], $m = 0.28$ eV, $\alpha = 56.6$ eV Å^2, $\alpha_z = 10.0$ eV Å^2, and $v = 4.1$ eV Å. The coefficient α_z drops from the ratio. The shadowed regions indicate the region around $v_z = 2.2$ eV Å that is realized in the undoped material. We clearly see that by decreasing v_z/v we can obtain negative b_2 values. The strong topological character of the material allows a wide range of variation of v_z through

doping, without changing the topological nature of the system, so that a chiral phase can be obtained by properly choosing the dopants and their amount.

V. CHIRAL PHASE IN THIN SLABS

In the 2D limit the Fermi surface is a line at $k_z = 0$, the coefficient b_2 Eq. (9) is explicitly negative, and the chiral phase is stable. The case $v_z \to 0$ and $\alpha_z \to 0$ is clearly realized when the system approaches the limit of quasi decoupled layers or the quasi-2D limit, characterized by an open Fermi surface [54]. We now study the stability of the nematic versus the chiral phase for reduced thickness of the sample by varying the number of unit cell layers.

We consider a simplified tight-binding model along the lines of Ref. [53]. We approximate the QL structure as a bilayer system (BL) composed by its top most (T) and bottom most (B) Se layers, described by triangular lattices on top of each other. The entire structure is described by the tight-binding Hamiltonian

$$H_{\rm TI} = H_0 + H_R + H_z. \tag{11}$$

The first term H_0 describes spin-independent hopping within the same layer and nearest-neighbor tunneling between the two layers,

$$H_0 = t_0 \sum_{\langle i,j\rangle,\sigma s} c^\dagger_{i,\sigma,s} c_{j,\sigma,s} + t_1 \sum_i c^\dagger_{i,T,s} c_{i,B,s} + \text{H.c.} + t_2 \sum_{\langle i,j\rangle,s} (c^\dagger_{i,T,s} c_{j,B,s} + c^\dagger_{i,B,s} c_{j,T,s}), \tag{12}$$

with $\sigma = T, B$ labeling the two layers. Atoms in the two layers experience local opposite electric fields along the $\pm\hat{z}$ direction that give rise to Rashba SOI of opposite sign on the two layers in the form

$$H_R = i\lambda \sum_{\langle ij\rangle\sigma,ss'} p_\sigma c^\dagger_{i,\sigma,s} c_{j,\sigma,s'} \mathbf{s}_{ss'} \cdot \hat{z} \times \mathbf{a}_{ij}, \tag{13}$$

with $p_{T,B} = \pm 1$ and $\mathbf{a}_{ij}$ a unit vector connecting site i and site j. Finally, along the z direction the structure is repeated as a series of tightly bound BL planes weakly coupled by van der Waals forces. Within the effective bilayer model the dynamics along the vertical direction can be described by an interlayer hopping term

$$H_z = t_z \sum_j c^\dagger_{j,T,s} c_{j-1,B,s} + \text{H.c.}, \tag{14}$$

with t_z intercell hopping amplitude.

The Hamiltonian $H_{\rm TI}$ describes a 3D TI, whose small momentum expansion well approximates the Hamiltonian Eq. (1) with in-plane velocity $v = 3\lambda a$, out-of-plane velocity $v_z = t_z a_z$, and a mass term that depends on the momentum, $m(\mathbf{k}) = 6t_2 + t_1 + t_z - 3t_2 a^2 k^2/2 - t_z a_z^2/2$, from which we extract $m = 6t_2 + t_1 + t_z$, $\alpha = 3t_2 a^2/2$, and $\alpha_z = t_z a_z^2/2$ appearing in Eq. (10). In order to study the stability of the chiral phase for the massive Dirac model Eq. (1) we choose values of the tight-binding parameters t_0, t_1, t_2, λ, and t_z in a way that the band structure is well described by a Dirac equation at small momentum. With the choice specified in Fig. 2 we obtain a mass $m = -0.2$ eV and velocities $v = 7.5$ eV Å and $v_z = -5.46$ eV Å. These values are on order of those provided in Ref. [15] and the resulting model well describes the complicate band structure of Bi_2Se_3 at low energy.

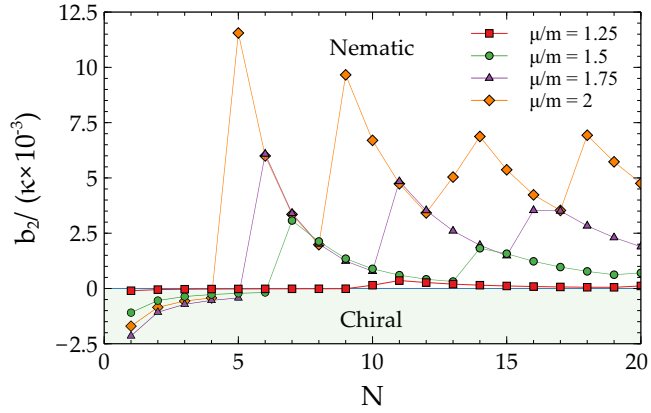

FIG. 2. Variation of the coefficient b_2 as a function of the number of layers N for different chemical potential. The parameter used in the tight-binding model are $t_0 = 0$, $t_1 = -4.1$ eV, $t_2 = 0.75$ eV, $t_z = -0.6$ eV, $\lambda = 0.5$ eV, $a = 5.0$ Å, and $a_z = 9.1$ Å.

The coefficient b_2 is calculated with the Fourier transformed Hamiltonian $H_{\rm TI}(\mathbf{k}_\parallel, n_z) = H_{\rm TI}(\mathbf{k}_\parallel, \pi n_z/N a_z)$, where N is the number of layers, and by collecting the relevant terms in the fourth-order expansion projected onto the conduction band

$$F_4 = \frac{\kappa}{N_F} \sum_{n_z,\mathbf{k}} \delta(\xi_{\mathbf{k},n_z}) \text{Tr}\left[\left(\mathcal{P}_{\mathbf{k},n_z} \Delta^\dagger \mathcal{P}_{\mathbf{k},n_z} \Delta\right)^2\right], \tag{15}$$

where $\mathcal{P}_{\mathbf{k},n_z} = \sum_{i=1,2} |\psi_{\mathbf{k},i}\rangle\langle\psi_{\mathbf{k},i}|$ is the projection operator of the conduction band subspace and $\Delta = -\psi_x \sigma_y s_y + \psi_y \sigma_y s_x$. We keep the tight-binding parameters fixed and only vary the number of layers N. In Fig. 2 we clearly see that the chiral phase is stable for sufficiently thin slabs of material. In particular, we see that the coefficient b_2 experiences quantum oscillations due to the coupling between the 2D layers. As a function of the chemical potential, small negative values of b_2 are obtained already for thick slabs and low doping, whereas larger negative b_2 values require higher doping and thinner slabs.

The coefficient b_2 follows the dispersion along the z direction. By reducing the number of layers the energy of the subbands grows and b_2 grows accordingly. As the energy of a given subband grows above the Fermi level the coefficient b_2 suddenly drops to the successive subband until a single band remains populated below the Fermi level. At that point b_2 becomes negative, as it cannot grow any longer. This explains why for low doping a structure composed by several unit cell develops the chiral phase, whereas for high doping one has to go down to the single layer case to encounter only one band below the Fermi level. The results of Fig. 2 are quite robust to variations of the tight-binding parameters characterizing the Hamiltonian, as long as the low-energy model is well captured by a massive Dirac Hamiltonian. The threshold N at which the transition to the chiral state takes place depends on the actual values of the tight-binding parameters. The quantum oscillations follow the band structure profile and they appear as long as the systems displays quantization of the subbands.

VI. CHIRAL MAJORANA MODES

The results presented in the previous sections show that a feasible way of obtaining a chiral phase is through exfoliation and that the extreme case of a single layer is the best candidate for chiral superconductivity. The chiral solution is given by $\boldsymbol{\psi} = \psi_0(1,i)$ so that the resulting gap on the Fermi surface reads

$$\Delta \propto \psi_0(k_y - ik_x)\tilde{s}_z, \tag{16}$$

where $\tilde{s}_z$ is the third Pauli matrix in the Kramers basis at momentum $\mathbf{k}$. Starting from the $k \cdot p$ Hamiltonian Eq. (1) at $k_z = 0$ we can write the Kramer basis by employing the manifestly covariant Bloch basis (MCBB) introduced in Refs. [34,52], where the band eigenstates are chosen to be fully spin polarized along the z direction at the origin of point group symmetry operations,

$$|\psi_{\mathbf{k},1}\rangle = \begin{pmatrix} \sqrt{\epsilon_k + m} \\ \sqrt{\epsilon_k + m} \\ ik_x - k_y \\ -ik_x + k_y \end{pmatrix}, \quad |\psi_{\mathbf{k},2}\rangle = \begin{pmatrix} -ik_x - k_y \\ ik_x + k_y \\ \sqrt{\epsilon_k + m} \\ \sqrt{\epsilon_k + m} \end{pmatrix}, \tag{17}$$

in the basis $(c_{\mathbf{k},T,\uparrow}, c_{\mathbf{k},B,\uparrow}, c_{\mathbf{k},T,\downarrow}, c_{\mathbf{k},B,\downarrow})^T$, up to a normalization factor $1/(2\sqrt{\epsilon_k^2 + m\epsilon_k})$. The action of time-reversal $\mathcal{T} = is_y K$, parity $\mathcal{P} = \sigma_x$, and mirror about x, $M_x = is_x$, are easily computed, resulting in the following transformation properties: $\mathcal{T}|\psi_{\mathbf{k},1}\rangle = -|\psi_{-\mathbf{k},2}\rangle$, $\mathcal{T}|\psi_{\mathbf{k},2}\rangle = |\psi_{-\mathbf{k},1}\rangle$, $\mathcal{P}|\psi_{\mathbf{k},i}\rangle = |\psi_{-\mathbf{k},i}\rangle$, and $M_x|\psi_{\mathbf{k},1}\rangle = i|\psi_{M_x\mathbf{k},2}\rangle$, $M_x|\psi_{\mathbf{k},2}\rangle = i|\psi_{M_x\mathbf{k},1}\rangle$. It is then clear that $|\psi_{\mathbf{k},1}\rangle$ and $|\psi_{\mathbf{k},2}\rangle$ form a Kramers doublet and represent a preferential basis that transform like a spin-1/2 object [52]. It is easily seen that the gap matrix $\Delta = \Delta_0(-\sigma_y s_y + i\sigma_y s_x)$ results in Eq. (16) when projected on the basis spanned by $|\psi_{\mathbf{k},1}\rangle$ and $|\psi_{\mathbf{k},2}\rangle$. At this point, the description in terms of the four-band original massive Dirac Hamiltonian can be substituted by a simpler description of the conduction band in the MCBB [52].

The BdG Hamiltonian Eq. (2) with the gap Eq. (16) projected onto the conduction band reads

$$H_{\mathrm{BdG}} = \begin{bmatrix} \xi_{\mathbf{k}} & \Delta(k_x - ik_y)\tilde{s}_z \\ \Delta(k_x + ik_y)\tilde{s}_z & -\xi_{\mathbf{k}} \end{bmatrix}. \tag{18}$$

The system breaks TRI and belongs to class D topological superconductors in 2D. A finite Chern number $C_{\mathrm{ch}} = \pm 2$ is easily calculated from Eq. (18), with the sign $\pm$ depending of whether the $(1,i)$ or $(1,-i)$ solution is realized. Correspondingly, two copropagating chiral Majorana modes are expected to localize at the edge of the system. This can be seen directly from inspection of Eq. (18). We see that both the spin-up and spin-down components are affected by a chiral $p_x + ip_y$ pairing, with gap of opposite sign for the two spin projections, due to the triplet nature of the pairing. Spinless chiral superconductivity in 2D opens a topologically nontrivial gap on the Fermi surface that gives rise to a single chiral Majorana mode at the boundary of the system, flowing with a velocity $v_M = \mp|\Delta|/k_F$, for the $p_x \pm ip_y$ cases, respectively. We then expect two chiral Majorana modes, each for spin component, that copropagate at the boundary of the system with $v_M = -|\Delta|/k_F$, with Δ the mean-field value of the order parameter ψ_0 in Eq. (16).

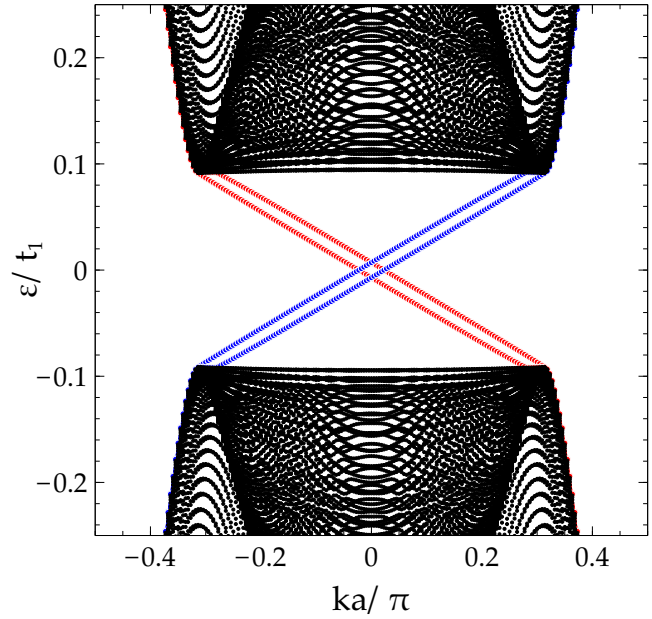

FIG. 3. Bands structure of a TI single layer with chiral superconductivity on a ribbon geometry. The parameters used are $t_0 = -0.1$, $t_1 = -5t_2$, $t_2 = 1.0$, $\lambda = 0.5$, $\Delta = 0.1$, and $\mu = 0.2$. Two Majorana edge states copropagate on each side of the ribbon (blue on one side, red on the other side).

In order to check the predictions of the low-energy effective model Eq. (18), we calculate the bands of the tight-binding model on a ribbon geometry. The mean-field Hamiltonian is $H_{\mathrm{MF}} = H_{\mathrm{TI}} + H_{\mathrm{SC}}$, with H_{SC} the Hamiltonian term describing superconductivity at mean-field level in the chiral phase,

$$H_{\mathrm{SC}} = \sum_{i;\sigma s,\sigma' s'} c^{\dagger}_{i,\sigma s} c^{\dagger}_{i,\sigma' s'} \hat{\Delta}_{\sigma s;\sigma' s'} + \mathrm{H.c.}, \tag{19}$$

with $\hat{\Delta} = \Delta\sigma_y(s_x + is_y)is_y$. The band structure on a ribbon geometry is shown in Fig. 3, where clear copropagating chiral Majorana modes appear, blue on one side and red on the other side of the ribbon.

VII. CONCLUSION

In this work we studied the stability of the chiral phase versus the nematic phase in Bi_2Se_3 as a function of the anisotropy of the system and the thickness of the sample. We showed that by increasing the two-dimensional character of the Fermi surface the chiral phase is expected to become stable. This can be experimentally achieved by properly choosing the doping element and their amount that by intercalation modify the interlayer distance and enhance the two-dimensional character of the system. A second root towards the realization of a chiral phase is achieved by exfoliation. We found that by reducing the number of layers constituting a thin slab of material the chiral phase can be stabilized already in few layer thick slabs and, for the low doping case, exfoliation down to $N < 10$ layer is expected to show the chiral phase. In particular, the single-layer case is shown to always favor the chiral phase. The resulting states is a chiral topological superconductor that hosts two copropagating chiral Majorana modes at its boundary. Our findings promote single layer of Bi_2Se_3 as an ideal material for

the manifestation of chiral superconductivity, opening the route to topological quantum computations with Majorana modes.

ACKNOWLEDGMENTS

The author acknowledges useful discussions with F. Finocchiaro, F. de Juan, and F. Guinea and he is thankful to J. Schmalian for a key comment on the role of Rashba SOI. This work is supported by the European Union's Seventh Framework Programme (FP7/2007-2013) through the ERC Advanced Grant NOVGRAPHENE (Grant No. 290846) and the Comunidad de Madrid through the Grant No. MAD2D-CM, S2013/MIT-3007.

[1] M. Sigrist and K. Ueda, Rev. Mod. Phys. **63**, 239 (1991).
[2] X.-L. Qi and S.-C. Zhang, Rev. Mod. Phys. **83**, 1057 (2011).
[3] N. Read and D. Green, Phys. Rev. B **61**, 10267 (2000).
[4] D. A. Ivanov, Phys. Rev. Lett. **86**, 268 (2001).
[5] J. Alicea, Rep. Prog. Phys. **75**, 076501 (2012).
[6] C. W. J. Beenakker, Annu. Rev. Condens. Matter Phys. **4**, 113 (2013).
[7] R. Aguado, Riv. Nuovo Cimento **40**, 523 (2017).
[8] T. Meng and L. Balents, Phys. Rev. B **86**, 054504 (2012).
[9] J. D. Sau and S. Tewari, Phys. Rev. B **86**, 104509 (2012).
[10] S. A. Yang, H. Pan, and F. Zhang, Phys. Rev. Lett. **113**, 046401 (2014).
[11] P. K. Biswas, H. Luetkens, T. Neupert, T. Stürzer, C. Baines, G. Pascua, A. P. Schnyder, M. H. Fischer, J. Goryo, M. R. Lees *et al.*, Phys. Rev. B **87**, 180503 (2013).
[12] M. H. Fischer, T. Neupert, C. Platt, A. P. Schnyder, W. Hanke, J. Goryo, R. Thomale, and M. Sigrist, Phys. Rev. B **89**, 020509 (2014).
[13] C. Nayak, S. H. Simon, A. Stern, M. Freedman, and S. Das Sarma, Rev. Mod. Phys. **80**, 1083 (2008).
[14] S. D. Sarma, M. Freedman, and C. Nayak, npj Quant. Inf. **1**, 15001 (2015).
[15] H. Zhang, C.-X. Liu, X.-L. Qi, X. Dai, Z. Fang, and S.-C. Zhang, Nat. Phys. **5**, 438 (2009).
[16] M. Z. Hasan and C. L. Kane, Rev. Mod. Phys. **82**, 3045 (2010).
[17] Y. S. Hor, A. J. Williams, J. G. Checkelsky, P. Roushan, J. Seo, Q. Xu, H. W. Zandbergen, A. Yazdani, N. P. Ong, and R. J. Cava, Phys. Rev. Lett. **104**, 057001 (2010).
[18] L. A. Wray, S.-Y. Xu, Y. Xia, Y. S. Hor, D. Qian, A. V. Fedorov, H. Lin, A. Bansil, R. J. Cava, and M. Z. Hasan, Nat. Phys. **6**, 855 (2010).
[19] M. Kriener, K. Segawa, Z. Ren, S. Sasaki, and Y. Ando, Phys. Rev. Lett. **106**, 127004 (2011).
[20] S. Sasaki, M. Kriener, K. Segawa, K. Yada, Y. Tanaka, M. Sato, and Y. Ando, Phys. Rev. Lett. **107**, 217001 (2011).
[21] N. Levy, T. Zhang, J. Ha, F. Sharifi, A. A. Talin, Y. Kuk, and J. A. Stroscio, Phys. Rev. Lett. **110**, 117001 (2013).
[22] H. Peng, D. De, B. Lv, F. Wei, and C.-W. Chu, Phys. Rev. B **88**, 024515 (2013).
[23] L. Fu and E. Berg, Phys. Rev. Lett. **105**, 097001 (2010).
[24] Shruti, V. K. Maurya, P. Neha, P. Srivastava, and S. Patnaik, Phys. Rev. B **92**, 020506 (2015).
[25] Z. Liu, X. Yao, J. Shao, M. Zuo, L. Pi, S. Tan, C. Zhang, and Y. Zhang, J. Am. Chem. Soc. **137**, 10512 (2015).
[26] Z. Wang, A. A. Taskin, T. Frölich, M. Braden, and Y. Ando, Chem. Mater. **28**, 779 (2016).
[27] T. Asaba, B. J. Lawson, C. Tinsman, L. Chen, P. Corbae, G. Li, Y. Qiu, Y. S. Hor, L. Fu, and L. Li, Phys. Rev. X **7**, 011009 (2017).
[28] K. Matano, M. Kriener, K. Segawa, Y. Ando, and G.-q. Zheng, Nat. Phys. **12**, 852 (2016).
[29] S. Yonezawa, K. Tajiri, S. Nakata, Y. Nagai, Z. Wang, K. Segawa, Y. Ando, and Y. Maeno, Nat. Phys. **13**, 123 (2016).
[30] Y. Pan, A. M. Nikitin, G. K. Araizi, Y. K. Huang, Y. Matsushita, T. Naka, and A. de Visser, Sci. Rep. **6**, 28632 (2016).
[31] M. P. Smylie, H. Claus, U. Welp, W.-K. Kwok, Y. Qiu, Y. S. Hor, and A. Snezhko, Phys. Rev. B **94**, 180510 (2016).
[32] J. Shen, W.-Y. He, N. F. Q. Yuan, Z. Huang, C.-w. Cho, S. H. Lee, Y. S. Hor, K. T. Law, and R. Lortz, npj Quantum Mater. **2**, 59 (2017).
[33] L. Fu, Phys. Rev. B **90**, 100509 (2014).
[34] J. W. F. Venderbos, V. Kozii, and L. Fu, Phys. Rev. B **94**, 180504 (2016).
[35] T. Hashimoto, K. Yada, A. Yamakage, M. Sato, and Y. Tanaka, J. Phys. Soc. Jpn. **82**, 044704 (2013).
[36] Y. Nagai and Y. Ota, Phys. Rev. B **94**, 134516 (2016).
[37] J. W. F. Venderbos, V. Kozii, and L. Fu, Phys. Rev. B **94**, 094522 (2016).
[38] F. Wu and I. Martin, Phys. Rev. B **95**, 224503 (2017).
[39] A. A. Zyuzin, J. Garaud, and E. Babaev, Phys. Rev. Lett. **119**, 167001 (2017).
[40] L. Chirolli, F. de Juan, and F. Guinea, Phys. Rev. B **95**, 201110 (2017).
[41] N. F. Q. Yuan, W.-Y. He, and K. T. Law, Phys. Rev. B **95**, 201109 (2017).
[42] F. Wu and I. Martin, Phys. Rev. B **96**, 144504 (2017).
[43] R. M. Fernandes, A. V. Chubukov, J. Knolle, I. Eremin, and J. Schmalian, Phys. Rev. B **85**, 024534 (2012).
[44] M. Hecker and J. Schmalian, npj Quantum Mater. **3**, 26 (2018).
[45] Y. Zhang, K. He, C.-Z. Chang, C.-L. Song, L.-L. Wang, X. Chen, J.-F. Jia, Z. Fang, X. Dai, W.-Y. Shan *et al.*, Nat. Phys. **6**, 712 (2010).
[46] G. Zhang, H. Qin, J. Chen, X. He, L. Lu, Y. Li, and K. Wu, Adv. Funct. Mater. **21**, 2351 (2011).
[47] M. S. Scheurer, D. F. Agterberg, and J. Schmalian, npj Quantum Mater. **2**, 9 (2017).
[48] A. P. Schnyder, S. Ryu, A. Furusaki, and A. W. W. Ludwig, Phys. Rev. B **78**, 195125 (2008).
[49] L. Chirolli, J. P. Baltanás, and D. Frustaglia, Phys. Rev. B **97**, 155416 (2018).

[50] F. Parhizgar and A. M. Black-Schaffer, Sci. Rep. **7**, 9817 (2017).
[51] S. Nakosai, Y. Tanaka, and N. Nagaosa, Phys. Rev. Lett. **108**, 147003 (2012).
[52] L. Fu, Phys. Rev. Lett. **115**, 026401 (2015).
[53] T. H. Hsieh and L. Fu, Phys. Rev. Lett. **108**, 107005 (2012).
[54] E. Lahoud, E. Maniv, M. S. Petrushevsky, M. Naamneh, A. Ribak, S. Wiedmann, L. Petaccia, Z. Salman, K. B. Chashka, Y. Dagan *et al.*, Phys. Rev. B **88**, 195107 (2013).